Tribology International 198 (2024) 109824

Contents lists available at ScienceDirect

Tribology International

journal homepage: www.elsevier.com/locate/triboint

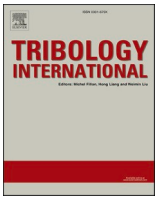

High-temperature tribological behaviour and machining performance of self-lubricant CrAlNAg coatings for dry milling operations

S.S. Rajput [a], C. Upadhyay [b], S. Gangopadhyay [a,*], F. Fernandes [c,d]

[a] Department of Mechanical Engineering, Indian Institute of Technology Bhilai, Durg 491001, Chhattisgarh, India
[b] Department of Mechanical Engineering, National Institute of Technology Rourkela, 769008 Odisha, India
[c] University of Coimbra, CEMMPRE, ARISE, Department of Mechanical Engineering, Rua Luís Reis Santos, 3030-788, Coimbra, Portugal
[d] CIDEM, ISEP, Polytechnic of Porto, Rua Dr. António Bernardino de Almeida, 431, 4249-015 Porto, Portugal

ARTICLE INFO

Keywords:
CrAlNAg coatings
Tribology
Self-lubricating
High-temperature
Face milling
Tool wear

ABSTRACT

Tribological and machining performance of CrAlNAg coatings having different Ag content tested against AISI 1045 medium carbon steel were assessed. Wear track was evaluated by scanning electron microscopy and energy dispersive spectroscopy. 3D topography of wear track and ball counterpart was determined by non-contact type profilometer. The formation of different oxide phases on track was confirmed using Raman spectroscopy. CrAlNAg9 and CrAlNAg12 coatings were found beneficial in reducing material adhesion from counterpart thus providing protective layers to counterpart, whereas small addition of Ag did not provide any improvement on CrAlN coating performance. CrAlNAg9 coated milling inserts demonstrated best results in terms of reduction in chip temperature (~17.5 %), cutting forces, surface roughness (~47 %) and chip thickness (~12.7 %) compared to uncoated inserts.

1. Introduction

With stringent environmental regulations, the industries in recent times are under greater obligation to minimize the usage of liquid lubrication in tribological applications. Machining industries, being the largest users of cutting fluids, are looking for more environment-friendly alternatives since machining involves greater friction, cutting force and heat generation. The excessive temperatures encountered during machining have negative effects on the material properties of cutting tools thus reducing tool lifespan and accelerating tool wear [1–3]. Consequently, cutting forces and mechanical vibration may increase, leading to unacceptable surface quality and increased power consumption due to the diminished effectiveness of cutting tools [4,5]. Therefore, it is crucial to manage cutting temperatures by optimizing cutting parameters and utilising cutting fluids. These cutting fluids form a thin layer at the tool-chip interface, thereby reducing friction and leading to superior performance. However, traditional flood cooling methods cause environmental and health risks due to the petroleum-based nature of the fluids used. While these methods offer good lubrication, they provide inadequate cooling due to their low thermal properties, despite consuming a large amount of fluid [6]. Additionally, excessive fluid usage creates additional cost burdens to the machining industry [7]. On the other hand, dry cutting offers the advantage of eliminating the need for fluids, thus avoiding environment and health risks. This also helps reduce equipment cost, cleaning, and disposal costs related to liquid lubricants. However, dry machining comes with its own drawbacks, including insufficient chip removal, accelerated tool wear, sudden breakage of the tool and diminished surface quality [8,9]. Especially during high-speed and dry machining operations, the cutting temperatures and stresses on the cutting edges are significantly high, leading to rapid tool wear and excessive heat generation [3,10]. Application of surface engineering in the form of deposition of hard coatings over the surface of the cutting tools allows them to extend their service life. TiC and TiN coatings were the early coating systems that were developed and applied to the protection of the cutting tools [11,12]. TiN coating along with other nitride coatings, was further alloyed with Al, to enhance their mechanical and thermal properties [13–16]. This alloying approach allowed to expand their applicability in turning, milling and drilling operations by offering improved oxidation resistance and thermal stability of the coating materials. Among these coating materials, metastable CrAlN is one of the prominent and widely adopted material systems in machining applications due to its excellent resistance to oxidation combined with superior mechanical and tribological properties [16–18]. In many cases, researchers found that CrAlN coating

* Corresponding author.
E-mail address: soumya@iitbhilai.ac.in (S. Gangopadhyay).

https://doi.org/10.1016/j.triboint.2024.109824
Received 20 April 2024; Received in revised form 13 May 2024; Accepted 23 May 2024
Available online 28 May 2024

outperforms the AlTiN coating in terms of improving the tool life (29 to 100 %), surface roughness (up to 16 %) and hardness (up to 147 %) [19,20]. Moreover, the formation of dense and adherent mixed oxides layer of Al and Cr ($(Al, Cr)_2O_3$) helps in the retardation of the oxidation process [20]. The properties of this nitride coating make it a popular choice for machining of engineering alloys such as different grades of steel.

AISI 1045 is a medium carbon steel extensively used in railway and automotive applications, as well as for fabrication of engine parts, couplings, and crankshafts [3,21]. Related industries prioritize high productivity, quality, cost efficiency and environmental waste reduction while machining AISI 1045 steel. In order to fulfill these demands, high-speed dry machining along with improved surface finish and tool life by reducing friction, existing coatings need some improvement by incorporating soft phase into their hard matrix. Addition of adequate quantity of soft phase such as Ag, into the matrix of nitride coatings, could be one of the strategies in the development of hard and solid lubricant coatings for cutting tools. Numerous research studies have concentrated on depositing transition metals nitride films with the addition of Ag [22–29]. Researchers who successfully incorporated Ag with CrN [27,30–32] and CrAlN [28] reported improvements in the tribological performance of the monolithic coatings (without Ag). As per the researchers, Ag diffuses on the top surface of the coating, during high-temperature tribology, forms a lubricious layer and helps easy sliding of the tribo-pair leading to reduction in friction [33]. The formation of oxides such as $AgCrO_2$, was found responsible for altering the oxidation and tribological behaviour of the coatings [26,34]. At elevated temperatures, these oxides are generated due to the migration of Ag on the top surface from within the coating under conditions of temperature exposure and sliding [26,34,35]. Therefore, the content of Ag within the nitride phase should be carefully controlled for achieving optimal combination of hardness and lubrication during tribology.

In this regard, Kutschej et al. [31] found that addition of 12 at.% of Ag into the matrix of CrN coating helped in maintaining a minimum coefficient of friction (~0.4) and depth of wear track (~1 μm) which was lower than monolithic CrN coating. However, increasing Ag up to 22 at. % in the same architecture resulted in reduction of the friction coefficient only during initial cycles, followed by coating failure during testing performed at 600 °C. The excessive outward diffusion of Ag from the coating initially provided lubrication, but over time, this phenomenon made the coating porous, rendering it incapable of withstanding forces during sliding, leading to failure. Other researchers working with a similar composition (22–25 at.%) of Ag in CrN reported coefficient of friction in the range of 0.2 to 0.7 while testing under a temperature ranging from 400 °C to 600 °C [30,32]. It was observed that the outward diffusion of Ag and the formation of bulk clusters helped reduce friction between sliding pairs. Previous researchers [26,36] indicated that doping Ag into CrAlN provided superior lubrication and resistance to wear both under room temperature and up to 600 °C compared with reference CrAlN coating.

In the previous work reported by the authors [26], it was identified that around 9 at.% of Ag was found effective in bringing about lowest coefficient of friction and specific wear rate than other Ag containing CrAlN-based coatings while sliding against Al_2O_3 ball. However, high-temperature tribological performance of Ag doped CrAlN coating against other counterparts remains relatively unexplored. Moreover, promising tribological performance of CrAlNAg coating also necessitates exploration of the capability of the same coating in machining applications. Therefore, the present research aims at investigating the tribological behaviour of CrAlNAg coatings with varying content of Ag against AISI 1045 steel ball counterpart. Attempt has been made to comprehensively understand the underlying mechanisms of friction and wear through tribological characterisation under high-temperature (600 °C) and evaluate the performance of CrAlNAg coatings in milling in terms of cutting force, chip temperature, surface finish and chip morphology in comparison with uncoated and reference CrAlN coated tools under dry environment.

2. Experimental procedure

2.1. Coating deposition and characterisation

The CrAlN coatings with different Ag concentrations were deposited using a 4-target coating system (Make: Teer coatings Ltd., UK) utilising closed-field unbalanced magnetron sputtering (CFUMBS) technique. A circular disk made of tungsten carbide (WC), with a diameter of 20 mm and a thickness of about 3.5 mm, was employed for tribology testing. Uncoated milling inserts (TPAN1603) manufactured by WIDIA, India were utilised as the other substrates to evaluate the machining performance of the coatings. Initially, the WC disks to be used for tribology were polished using 400, 600, and 800 grit SiC papers, followed by diamond paste with particle sizes of 3 μm and 0.8 μm, successively. This process aimed to maintain the surface roughness of all samples below 100 nm. Achievement of such a low value of surface roughness (R_a) was essential to ensure a uniform thickness of the coating all over the substrate. Subsequently, both sets of substrates were ultrasonically cleaned in separate baths of ethanol and acetone for 20 min each, followed by drying in an oven. To eliminate any remaining contaminants, the samples underwent etching with Ar^+ in the deposition chamber for 20 min under a base pressure of 4×10^{-6} Pa with an applied bias voltage of −600 V. The Ag concentration was adjusted by varying the power applied to the respective targets. Following deposition, the coated disk was cut to examine the fractured cross-section, allowing for the analysis of coating thickness and morphology using field emission scanning electron microscopy (FESEM Gemini500; Zeiss, Germany) with the attachment of energy dispersive spectroscopy (EDS). For comprehensive details related to the deposition of the coatings, their mechanical and structural characterisation, as well as their oxidation resistance at elevated temperature, readers are referred to the previous work of the authors [26,34]. A summary of the chemical composition and the coating properties relevant to this research work is provided in Table 1 [34].

2.2. Tribological characterisation

The tribological performance of the coatings was analysed at 600 °C utilising a ball-on-disk type tribometer (CSM Instruments). The tests were conducted according to ASTM G99–17 standard utilising an AISI 1045 medium carbon steel ball (6 mm diameter). The ball has a composition of 98.5 to 98.97 % iron (Fe), 0.60 to 0.9 % manganese (Mn), ≤ 0.04 % phosphorus (P) and ≤ 0.05 % sulphur (S) respectively. The same material was further used to perform the machining tests. It was

Table 1
Classification of coatings with their elemental composition, thickness and mechanical properties [34].

Samples	CrAlN	CrAlNAg2	CrAlNAg9	CrAlNAg12	CrAlNAg16
Coating thickness (μm)	2.5 ± 0.04	2.6 ± 0.08	3.0 ± 0.05	3.1 ± 0.05	3.3 ± 0.09
Cr (at.%)	37 ± 0.4	36 ± 0.8	34 ± 0.65	32 ± 0.5	31 ± 0.30
Al (at.%)	10.9 ± 0.2	10.4 ± 0.2	9.9 ± 0.1	9.3 ± 0.2	9.1 ± 0.08
N (at.%)	50.0 ± 0.4	48.8 ± 0.23	45.7 ± 0.18	44.1 ± 0.2	42.1 ± 0.25
Ag (at.%)	0.0	2.4 ± 0.1	8.6 ± 0.2	11.8 ± 0.22	15.8 ± 0.32
O (at.%)	2.1 ± 0.08	1.9 ± 0.09	1.7 ± 0.09	2.0 ± 0.06	1.8 ± 0.08
Cr/Al ratio	3.4 ± 0.1	3.5 ± 0.11	3.4 ± 0.1	3.5 ± 0.1	3.4 ± 0.12
Hardness (GPa)	18.0 ± 3.2	17.0 ± 2.6	23 ± 3.3	19.9 ± 3.3	14.4 ± 3.1

ensured that the chemical composition of the ball counterpart closely matched with that of the workpiece material. Some of the essential mechanical properties related to workpiece material are provided in Table 2. The tests were carried out at 600 °C with a 2 N load, 0.1 m/s linear speed and 6 mm track radius for 1250 cycles. The parameters were selected in such a way as to ensure the survival of the coatings even after the running-in period so that reasonable comparisons could be required during the steady-state regime. Moreover, the normal load was chosen in such a way that the contact condition in terms of Hertzian contact pressure during tribology as well as machining test could be maintained in a comparable range [37]. All the tests were repeated thrice for ascertaining the repeatability of the results. During the test, the required temperature was achieved by the muffle furnace attached to the tribometer, which was controlled by the thermocouple present inside the chamber at three different locations. Meanwhile, the coefficient of friction was continuously measured with the computer system integrated with the tribometer. After the test, samples were cooled inside the furnace itself. Developed wear track and ball counterparts from the tests were examined utilising a non-contact type surface profilometer (S neox; Sensofar, Spain). Following the tribological tests, the morphology of the wear track alongside the ball counterpart was analysed using FESEM, while the compositions of the sliding wear debris were determined utilising EDS. Raman spectroscopy (alpha300 R; WITec, Germany) equipped with an Ar laser operating at a wavelength of 532 nm was employed to scrutinize the wear track and its constituents.

2.3. Performance evaluation in dry machining

The current study aims at exploring the advantages of incorporating solid lubrication with hard nitride coating to enhance material removal rate (MRR) under severe conditions (combination of high cutting, feed and depth of cut) during dry milling operations. Considering the wide range of applications and extensive necessity of machining operations, AISI 1045 steel has been chosen as the workpiece material in the current research work. The shape of the workpiece was in the form of rectangular block with a dimension of 120 mm × 50 mm x 50 mm. Fig. 1 illustrates the experimental setup for face milling operation. Table 3 presents attributes regarding the cutting tools and conditions. The machining tests were carried out using a 3-axis vertical machining center (AMS 540 V: Ace Micromatic, India). All experiments were conducted in a dry environment to evaluate the machining performance of both uncoated and coated tools. To enhance the statistical accuracy of measuring various machining characteristics, all the experiments were repeated three times. The study examined the impact of different percentages of Ag in coatings on various machining characteristics during the face milling of AISI 1045 steel. The machining characteristics included the calculation of cutting force, surface roughness, chip temperature, tool wear (rake and flank wear) and chip characteristics.

2.4. Force and temperature analysis

To measure the cutting forces generated during cutting, a multicomponent (9257B; Kistler, Switzerland) dynamometer was used. The dynamometer was connected to a charge amplifier (5001 A; Kistler, Switzerland) having eight-channels and a data logger system. The combined arrangement facilitates the recording of data concerning the X, Y and Z components of cutting forces (F_x, F_y, and F_z, respectively) throughout the machining operation. Chip temperature was measured using an infrared (IR) camera (X6540sc; FLIR, US), calibrated to measure temperatures ranging from 350 °C to 1200 °C. During temperature recording the emissivity of the workpiece was assumed to be ~0.8 which was determined through a number of calibration experiments. Adapted methodology for measuring cutting temperature has been previously employed by other researchers as well [3,40].

Table 2
Mechanical and other properties of AISI 1045 steel [38,39].

Mechanical properties	Poisson's Ratio	0.3
	Elastic Modulus (GPa)	200
	Brinell Hardness	170-210
	Tensile Strength (MPa)	570-700
Other properties	Thermal Conductivity (W/(mK))	38
	Density (kg/m^3)	7800-7850

2.5. Wear analysis

Average flank and crater wear were determined after every five passes of the machining using a stereo-zoom microscope (S9i; LEICA, Germany). This allowed for the assessment of tool wear during machining with different uncoated and coated inserts. Machining operations were carried out for a total of 22 passes across all coating conditions, ensuring a comprehensive comparison of different machining characteristics including tool wear. Meanwhile, both the flank and rake surfaces of the tool inserts were inspected using SEM and EDS after completing 22 passes of face milling.

2.6. Chip thickness and surface roughness

Chip thickness and surface roughness are important characteristics for assessing machining performance. Surface roughness tests were conducted on the uncoated and as-deposited milling inserts and later on the machined workpiece using a portable roughness tester (Surtronic S-100; Taylor and Hobson, England) with a cut-off length of 0.8 mm and a sampling length of 4 mm. The parameter considered for surface roughness analysis was the arithmetic mean surface roughness (R_a). The stereo-zoom microscope was used to capture the optical images of the machined chips. The thickness of these chips was measured at their maximum cross-section with the help of a micrometer (C/N 342–251-30; Mitutoyo, Japan) having the least count of 0.01 mm. To ensure statistical accuracy, at least five repetitions were conducted, ensuring a reliable assessment of the surface roughness and chip thickness.

3. Results

3.1. Coatings thickness and surface roughness

The fractography technique was utilised to examine the thickness of the developed CrAlN and CrAlNAg coatings. Fractographs of the coatings, as a function of the chemical composition, are depicted in Fig. 2(a). The reference CrAlN coating demonstrates a smooth and uniform appearance, displaying a growth pattern involving a columnar cross-section. To enhance the adhesion of the coating with the WC substrate, an interlayer of Cr with a thickness of approximately 600 nm was first deposited for all the coating configurations. As Ag was introduced by increasing the power density applied to the Ag target during the deposition (maintaining the same power densities of Cr and Al targets as in the reference CrAlN coating), an increase in the coating thickness was observed, as evident from Fig. 2(a). The columnar structure was evident in all the deposited coatings. A representative image of elemental mapping (see Fig. 2(b)) carried out at the cross-section of the CrAlNAg9 coating reveals the distribution of different elements along the thickness of the coating.

The surface roughness of the uncoated milling insert was 0.293 μm, while that of the coated inserts is as follows.

CrAlN: 0.312 μm, CrAlNAg2: 0.305 μm, CrAlNAg9: 0.287 μm, CrAlNAg12: 0.268 μm, and CrAlNAg16: 0.261 μm.

Evidently, doping of Ag into the matrix of CrAlN was effective in bringing down the surface roughness, an observation that was also reported earlier [26].

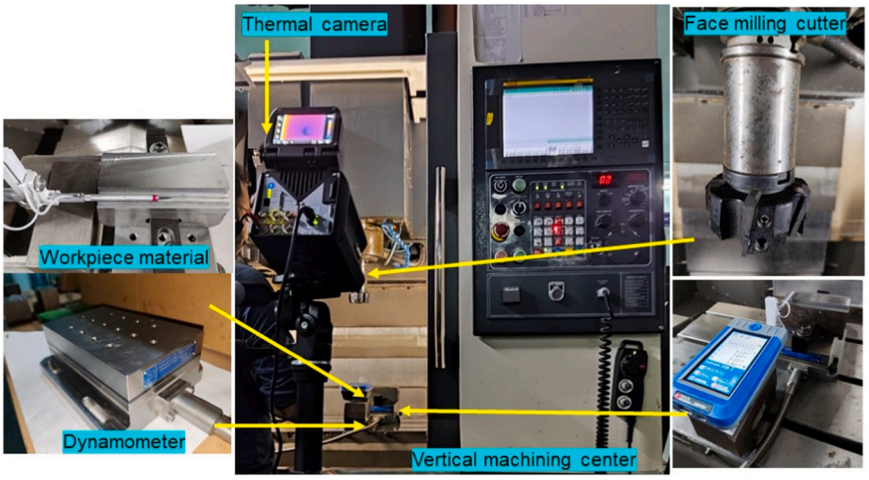

Fig. 1. Experimental setup for carrying out machining tests using uncoated and coated milling inserts.

Table 3
Specifications of cutting tools, workpiece and machining parameters for milling experiment.

Workpiece material	AISI 1045 medium carbon steel
Insert designation	TPAN 1603PPN THM
Inserts used	Uncoated cemented carbide inserts (ISO K10) Coated cemented carbide inserts: CrAlN, CrAlNAg2, CrAlNAg9, CrAlNAg12, CrAlNAg16
Tool holder	Face-mill cutter with BT-40 taper 85 mm diameter (Make: WIDIA)
Cutting velocity; V_c (m/min)	250
Feed; f_r (mm/min)	300
Feed/tooth; f_z (mm/tooth)	0.3205
Radial depth of cut; a_e (mm)	20
Axial depth of cut; a_p (mm)	1
No. of passes	22
Length of cut per pass (mm)	120
Environment condition	Dry

3.2. Tribological behaviour of coatings at 600 °C

Variations in the coefficient of friction versus sliding distance for all the coatings tested against AISI 1045 steel ball at 600 °C were presented in Fig. 3. The temperature and counterpart were intentionally selected to simulate the temperature generation during milling of AISI 1045 steel. The 3D profilometric image of the coated disk and counterpart steel ball are presented in Fig. 4. At 600 °C, the steel ball was softened and exhibited wear when sliding against the hard coating, as depicted in Fig. 4. Coatings with no Ag or low percentage of Ag doping demonstrated a significant amount of adhesion between the coating and counterpart, resulting in prominent wear flats. Conversely, the CrAlNAg9 and CrAlNAg12 coatings exhibited no sticking on the track.

Optimal Ag-doped coatings were found to form a protective transfer layer on top of the counterpart, enabling smooth gliding of the ball and minimizing direct contact with the disk, thus reducing wear. However, the CrAlNAg16 coating with the highest Ag content displayed a non-functional transfer layer on the counterpart, accompanied by a wear flat (Fig. 4). The excessive presence of softer Ag in the coating promoted uncontrolled outward diffusion, depleting the Ag content within a few cycles. This excessive diffusion led to the formation of a large and unsustainable transfer layer that was eventually removed during sliding. Consequently, the steel ball came into direct contact with the sliding track surface, resulting in metal deposition. This phenomenon explains why the coefficient of friction for CrAlN, CrAlNAg2, and CrAlNAg16 coatings is similar to that for iron-to-iron sliding, as observed in previous studies [41,42]. Notably, the presence of additional hard ceramic particles (Cr and Al, based) in the CrAlNAg12 coating increased the coefficient of friction. The CrAlNAg9 coating exhibited double track formation, which occurs when a hard particle from either the coating or counterpart (in this case, from the coating) becomes trapped in the track, leading to three-body abrasion [43,44]. Due to the particle's small size, it acts as a sharp pin sliding along the track, intensifying the conditions for the coating and resulting in increased wear depth. Consequently, the CrAlNAg9 coating displayed a higher coefficient of friction.

Fig. 5 displays the wear flat diameter and the maximum thickness of the transfer layer formed on several coatings. It is evident from the figure that CrAlN and CrAlNAg2 exhibit similar wear flat sizes, while the wear flat size for CrAlNAg9 is minimum and increases gradually thereafter. Regarding transfer layer thickness, no transfer layer was observed for CrAlN and CrAlNAg2 coatings. However, both CrAlNAg9 and CrAlNAg12 coatings developed a sustainable transfer layer. Conversely, the formation of a thick transfer layer in the CrAlNAg16 coating rendered it unsustainable during sliding.

Furthermore, the wear track was 2D scanned to examine the wear depth profile of the track, as shown in Fig. 6. It is clear from the figure that material sticking occurred on the wear track of CrAlN and CrAlNAg2 coatings. However, a unique double-track formation was observed for the case of the CrAlNAg9 coating. Whereas the wear depth suggested that substrates were exposed for the case of CrAlNAg12 and CrAlNAg16 coatings.

SEM and EDS mapping were conducted on both the wear track and ball counterpart to analyse their elemental composition. EDS analysis of the wear track, shown in Fig. 7, revealed the deposition of material from the ball counterpart onto the tracks of CrAlN and CrAlNAg16 coatings, primarily in the form of iron oxides. The presence of a double-track formation on the CrAlNAg9 coating indicated a deficiency of Ag within the wear depth. It is likely that aluminium oxide was also formed during sliding. The CrAlNAg16 coating displayed a decrease in Ag content within the track due to excessive outward diffusion. The elemental analysis of the wear tracks confirmed the deposition of iron oxide onto the wear tracks of reference CrAlN, CrAlNAg2 and CrAlNAg16 coatings. The track of the CrAlNAg9 coating did not show any evidence of worn particles comprising steel (iron) coming from the ball counterpart. The coating was primarily intact with the possible formation of oxides of Cr and Al (as evident from the elemental mapping of O) as the protective layer within the wear track. When considering the CrAlNAg16 coating, depletion of Ag within the track along with material

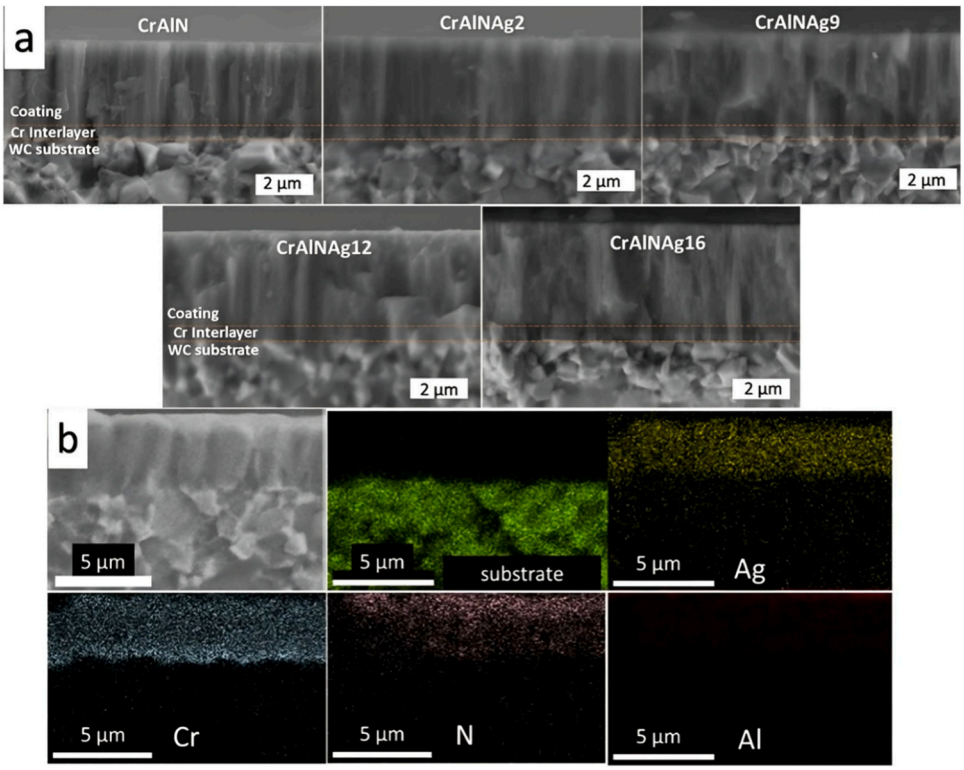

Fig. 2. (a) SEM micrographs of cross-section of coated CrAlNAg with different contents of Ag deposited over WC substrate along with (b) representative images of elemental mapping of CrAlNAg9 coating.

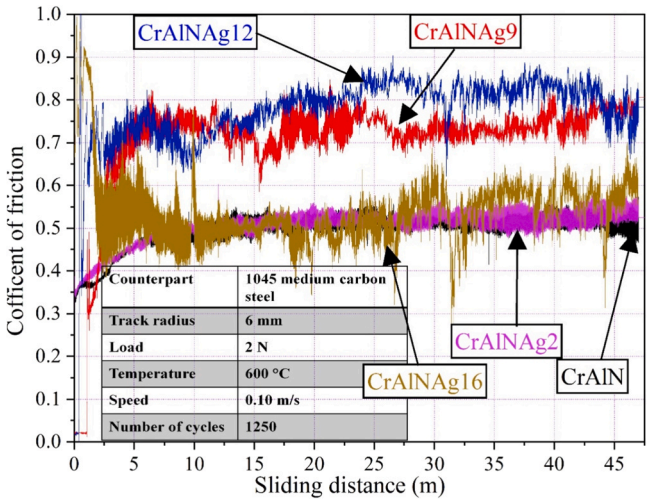

Fig. 3. Variation of coefficient of friction of CrAlNAg coatings when sliding against AISI 1045 steel ball at 600 °C.

adhesion (steel) was observed. The material adhesion could be attributed to significant ball wear as evident in Figs. 4 and 5. Wear of the ball counterpart caused the widening of the wear tracks for CrAlN, CrAlNAg2 and CrAlNAg16 coatings. It is noteworthy to mention that wearing of the counterpart ball for the case of CrAlN, CrAlNAg2 and CrAlNAg16 coatings increased the contact area and hence widening of the wear track took place.

For further analysis, Raman spectroscopy (please refer to Fig. 8) was conducted inside the wear track of the coatings, revealing the presence of Cr_2O_3, Fe_2O_3, Al_2O_3 and $AgCrO_2$ within the track. It is worth noting that the acceleration of local oxidation was attributed to the presence of defects induced by the sliding action [45]. Inside the wear track of the CrAlN coating, Al_2O_3 and Fe_2O_3 were observed, while no traces of Cr_2O_3 were found. The dominant peaks of Al_2O_3 were observed in the CrAlNAg12 coating, consistent with findings from a previous study [26]. The oxide phase of Ag ($AgCrO_2$) was significantly present in CrAlNAg16, followed by CrAlNAg12. CrAlNAg9 coated samples also exhibited the presence of Cr_2O_3, Al_2O_3 and $AgCrO_2$, but in lesser quantities compared to CrAlNAg12. It is important to note that this phase is thermally stable between the temperature range of 450 °C to 850 °C [29]. The generation of $AgCrO_2$ and the availability of Ag inside the sliding tracks contribute to the facilitation of sliding for the counterpart, as both are known for their low shearing properties [35,46]. However, excessive formation of $AgCrO_2$ can degrade the strength of the coating, as it occupies the surface and reduces the formation of the protective oxide layer (Cr_2O_3) on top of the coating.

EDS analysis of the ball counterpart, presented in Fig. 9, reveals no transfer layer formation for the CrAlN coating, with only abrasive wear of the ball occurring due to the harder CrAlN phase. The EDS elemental mapping also indicates a transfer layer rich in oxides of Cr and Al for CrAlNAg9 and CrAlNAg12 coatings. For the CrAlNAg9 coating, the presence of Ag in the transfer layer was not significant. Therefore, it can be concluded that the protective transfer layer was hard and abrasive, but without lubricious properties. As a result, the CrAlNAg9 coating exhibited a high coefficient of friction, apart from minor wear of the coating at the narrow point of contact between the oxides-rich transfer layer and the wear track. A larger area of the transfer layer in CrAlNAg12 and CrAlNAg16 caused greater depth of wear in the track. Although Ag was present in the transfer layer as shown in Fig. 9, it was segregated along the boundary of the transfer layer, while Al and Cr oxides formed in the areas of contact with the track. The segregation or accumulation of Ag took place along the boundary of the contact area of the ball counterpart as an outcome of outward diffusion of Ag from within the coating at high temperature leading to loss of lubricating phase (Ag) from the coating. A similar observation was also noted in the previous studies [47–50]. Therefore, Ag could not provide a major

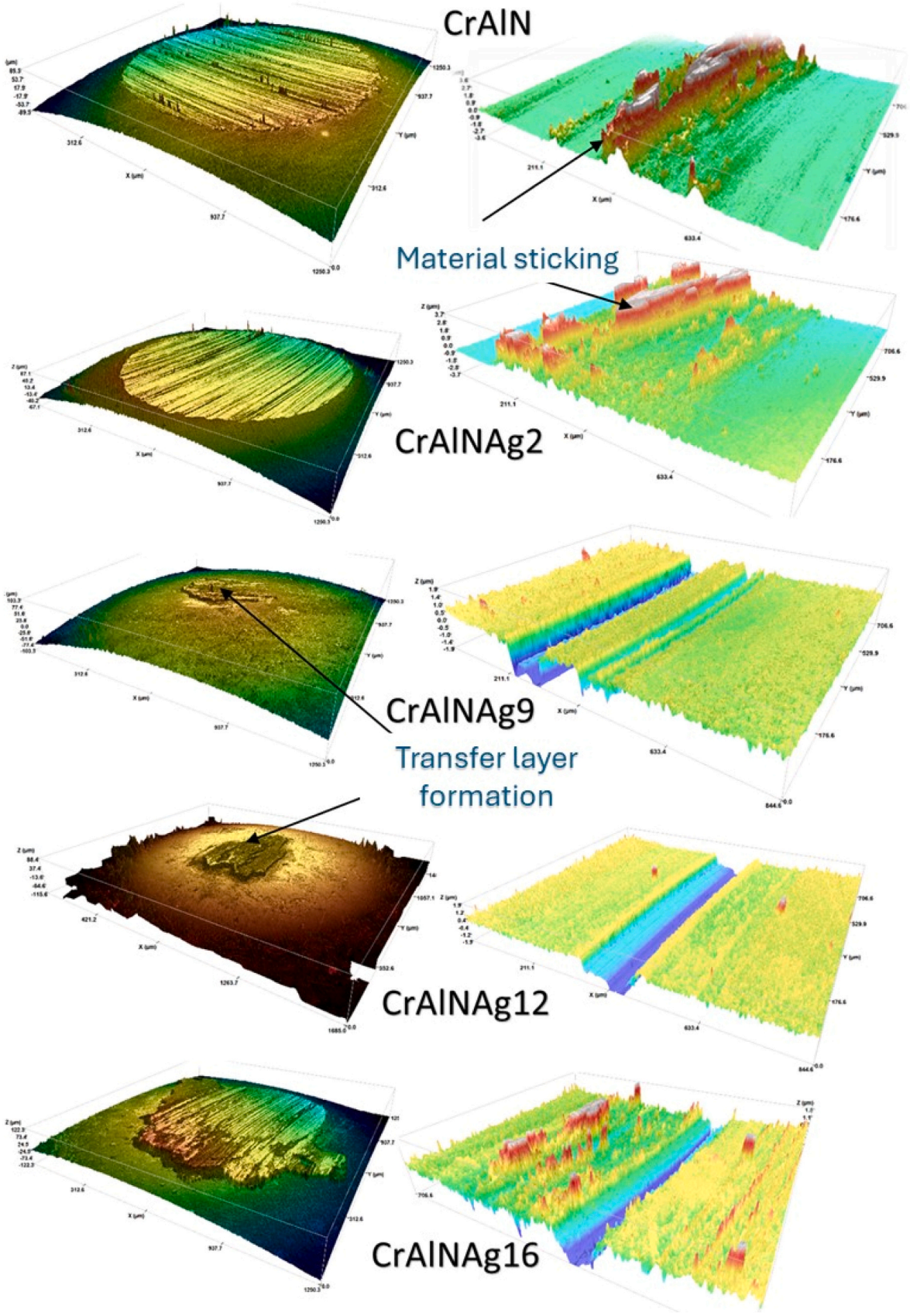

Fig. 4. 3D surface profilometer images of ball counterpart and wear track of CrAlNAg coatings after sliding against AISI 1045 steel ball at 600 °C.

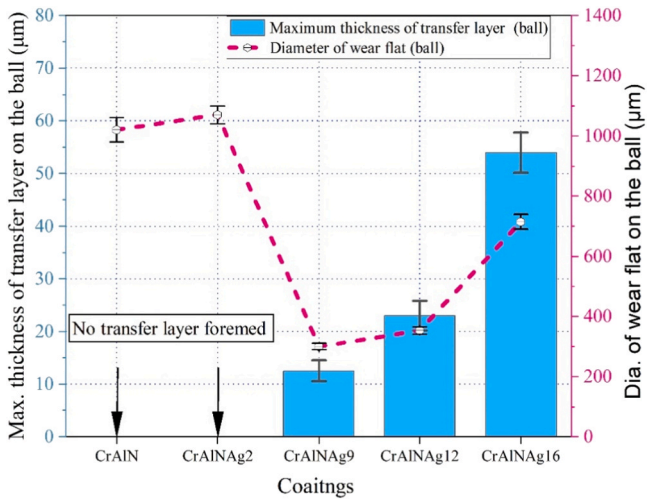

Fig. 5. Wear flat diameter and thickness of transfer layer after sliding against AISI 1045 steel ball at 600 °C.

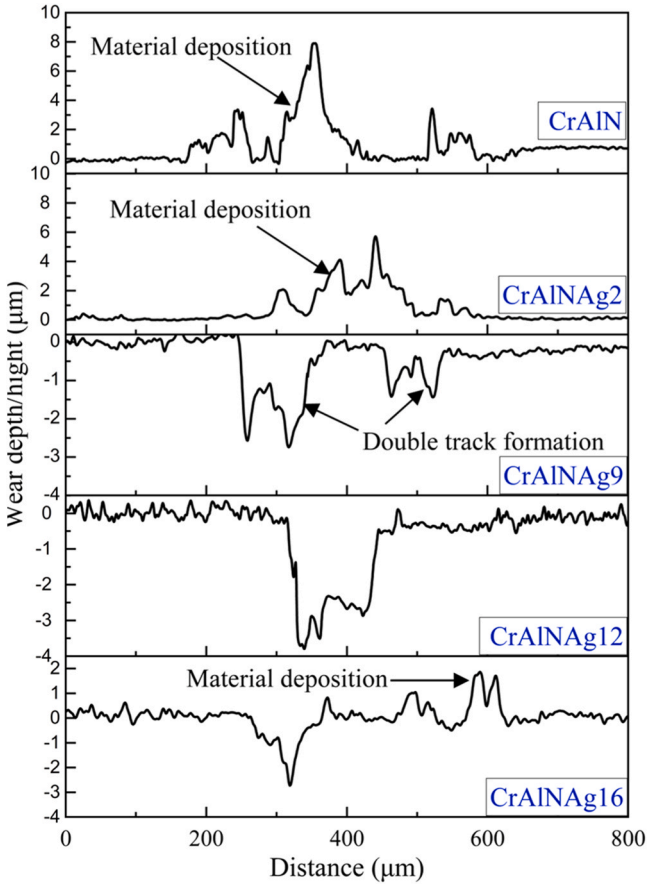

Fig. 6. Wear track profile (2D) of CrAlNAg coatings after sliding against AISI 1045 steel ball at 600 °C.

lubrication effect, and coating wear was more pronounced for CrAlNAg12 and CrAlNAg16 coatings.

3.3. Milling performance of the coating

During the face milling operation of AISI 1045 medium carbon steel, three cutting force components (F_x, F_y, F_z) were recorded. Fig. 10 (a) illustrates three such representative force profiles while machining with uncoated and CrAlNAg9 coated milling inserts. It is evident that the highest force (F_x) was generated along the direction of the table feed, while the lowest force (F_z) was observed along the cutter axis. In selected cutting parameters, radial depth is less than $1/4^{th}$ of the cutter diameter. Moreover, considering high material removal rate as an objective, the chosen feed per tooth was high. This resulted in higher cutting force along the feed direction. These could be the reasons for the recorded distribution of cutting forces. As the tool moves along the feed direction, it engages with the workpiece material, leading to the shearing and removal of material. The cutting edge of the tool meets the material at a specific angle known as the shear angle. This angle is influenced by both tool geometry and the properties of the material being cut. This shear angle significantly influences the component of cutting force along the feed direction.

The same Fig. 10 (b) also presents the variation of F_x, F_y, and F_z including maximum, minimum and mean values calculated from the cutting force profile for uncoated, CrAlN and CrAlNAg coated tools. It is noteworthy to mention that forces are being demonstrated only during the first pass of machining to negate the influence of tool wear. Uncoated milling inserts exhibit higher cutting force, particularly in terms of F_x and F_y, than CrAlN and CrAlNAg coatings. This is attributed to the anti-friction properties of the same coatings. While investigating the relative performance of the coated tools, it is observed that CrAlNAg12 coating resulted in higher values of F_x, F_y, and F_z than CrAlN and other CrAlNAg coatings.

In-depth analysis of high-temperature tribology results (Figs. 3 and 7) also pinpointed the inferior tribological performance of CrAlNAg12 coating in terms of higher friction, material adhesion and greater depth of wear track. Therefore, the results of cutting force are in agreement with those of tribology using the same counterpart as that of the workpiece material. Interestingly, CrAlNAg9 and CrAlNAg16 showed a reduction (6–12 %) in F_z compared to CrAlN, indicating the effectiveness of the addition of Ag into the hard CrAlN phase.

Fig. 11 illustrates the variation in chip temperature and the progression of chip temperature with each pass of milling. A total of 22 passes or until tool failure were considered. It is evident that the uncoated tool generated the highest temperature during machining. As the higher cutting force for the uncoated tool was associated with higher chip-tool interface friction, the same mechanism of greater frictional heat generation could explain the chip temperature. Since the uncoated tool failed after only 6 passes, the machining was discontinued for the same tool. The CrAlN coating imparted both anti-friction properties as well as wear resistance, resulting in a reduction in chip temperature. The benefit of the addition of Ag of an optimal quantity was evident as the CrAlNAg9 coating was effective in bringing down chip temperature in the range of 3–4 % compared to those of the CrAlN coating and 14–17 % compared to those of the uncoated tool. It is also evident that a very low content of Ag (2 %) was insufficient to provide a sizable lubrication effect for the CrAlNAg2 coating, whereas higher Ag content was also not effective. CrAlNAg12 exhibited poor tribological behaviour all along, resulting in a higher chip temperature than those for the CrAlN, CrAlNAg2, and CrAlNAg9 coatings. A little consideration would indicate that the chip temperature for the CrAlAg16 coating was similar to that of the CrAlNAg9 coating after 2 passes. However, owing to excessive outward diffusion of Ag to the surface followed by loss, the CrAlAg16 coating quickly lost its tribological properties and as a result, it suffered from a higher rate of tool wear (to be discussed later) and escalated the rise in chip temperature. The sharpest slope of increase of chip temperature is comparable only with the uncoated tool.

The condition of those tools after 22 runs of face milling under dry conditions is depicted in Fig. 12 using SEM images. The figure reveals that the uncoated tool suffered from breakage of the cutting edge and nose, indicating severe wear. Whereas, higher material adhesion could be observed for CrAlN coated inserts. Apart from adhesion, the CrAlN coated tool also suffered from edge chipping but with much less severity than the uncoated tool. The high brittleness of the CrAlN coated tool was

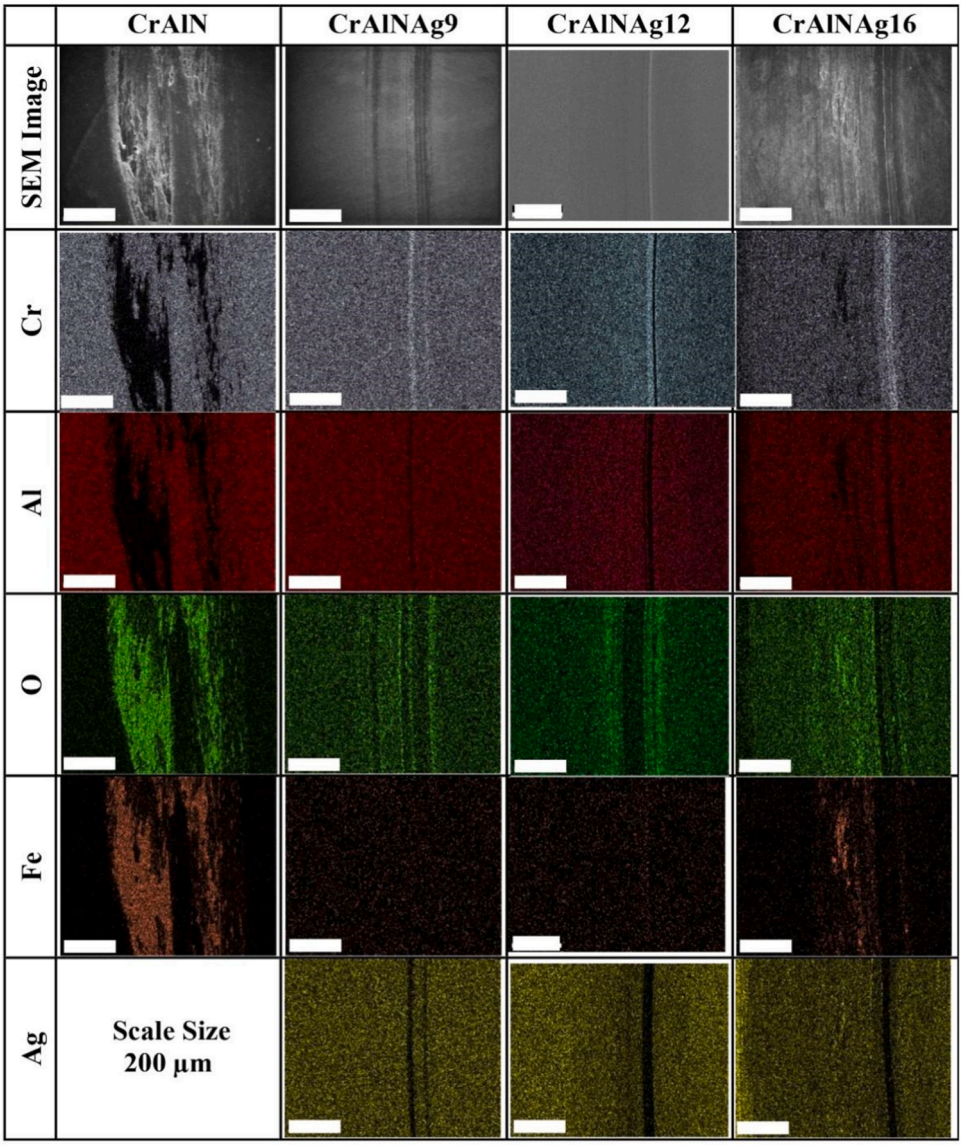

Fig. 7. SEM and EDS elemental mapping images of wear track of CrAlNAg coatings tested against AISI 1045 steel ball at 600 °C.

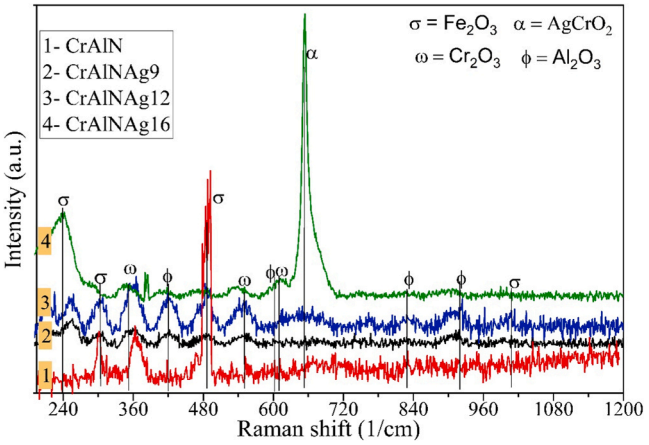

Fig. 8. Raman spectra of the wear track of CrAlNAg coatings after sliding against AISI 1045 steel ball at 600 °C.

not effective in withstanding the high force and stress of aggressive machining conditions. The inclusion of the softer phase of Ag was of clear benefit in terms of improving resistance to edge chipping of the tool.

The superior tribological properties of CrAlN and CrAlNAg9 coatings compared to the other coatings were also found to correlated with the tool wear phenomena. Higher resistance to tool wear of CrAlNAg9 coating in comparison with reference CrAlN coated tool is attributed to higher coating hardness of CrAlNAg9 coating than CrAlN as shown in Table 1. While the uncoated insert suffered from severe wear characterised by escalated nose damage (with an average wear band of 77 µm) and crater wear (with an average depth of 9 µm) after only 6 passes, the other coatings survived for 22 runs. Various wear mechanisms could also be observed, including edge chipping and material adhesion over the CrAlN coated tool, crack formation at the rake surface of the CrAlNAg16 coating, etc.

The average flank wear was periodically measured after a finite number of milling passes so that the progressive wear of the uncoated and coated tools could be investigated. The results are demonstrated in Fig. 13, in which it is evident that the minimum flank wear could be accomplished with the CrAlNAg9 coated tool, followed by CrAlNAg2 and CrAlN coated tools. However, it may be noted that this reduction in

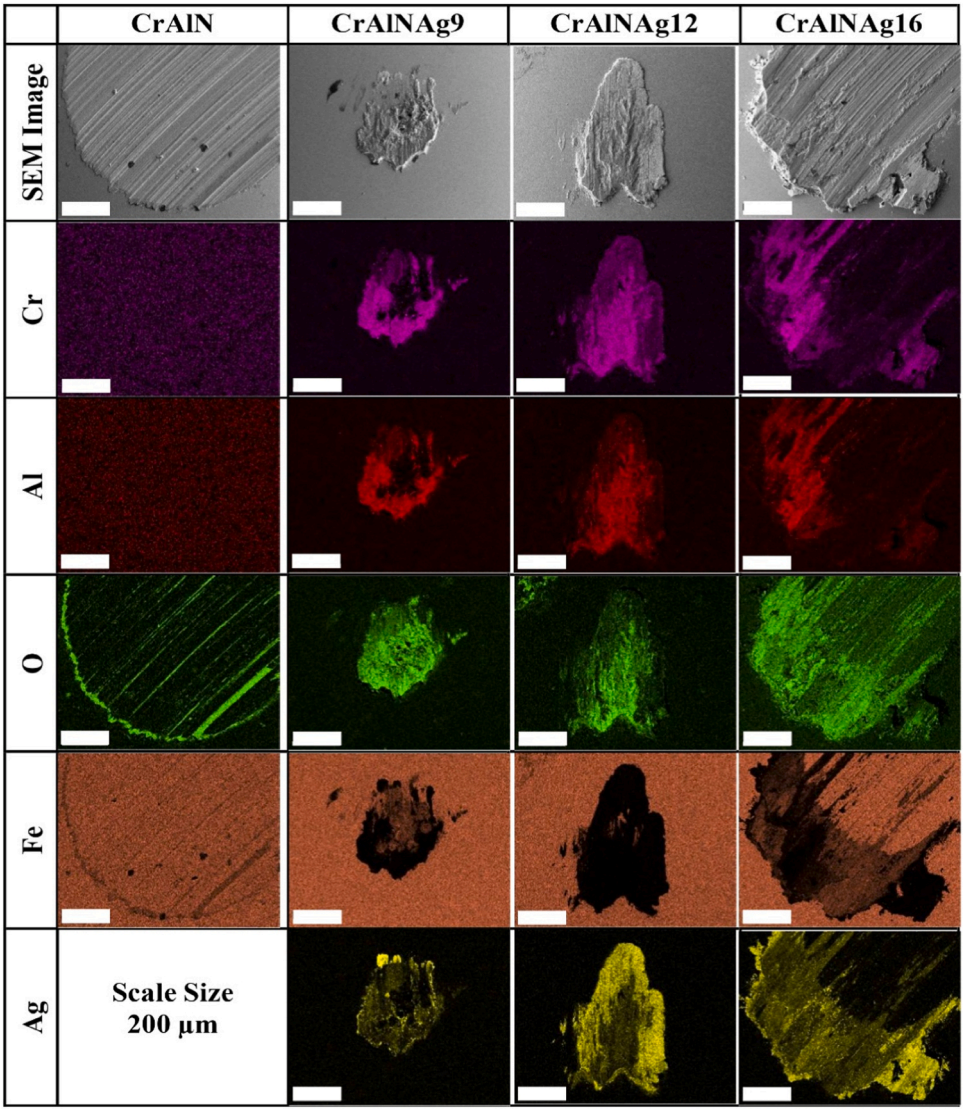

Fig. 9. SEM and EDS elemental mapping images of AISI 1045 steel ball counterpart after sliding against CrAlNAg coatings tested at 600 °C.

flank wear was in the range of 7–10 %. This result is in agreement with those of cutting force and chip temperature as no significant improvement was received with the addition of Ag. Moreover, CrAlNAg12 and CrAlNAg16 coated tools showed greater flank wear. It is noteworthy to mention that the lower values of flank wear are attributed to the geometry of the milling inserts having a chamfered cutting edge. Therefore, the flank surface is protected until the chamfered edge gives in. The tool will therefore fail even with the lower values of flank wear if the chamfered edge suffers from severe damage leading to chipping or breakage of the cutting edge and nose [3,51]. This is exactly what has been observed in the current research work. A similar trend was also followed in the progressive depth of crater wear (shown in Fig. 14) for the uncoated and coated tools. CrAlN, CrAlNAg2, and CrAlNAg9 coatings showed similar crater wear (with a depth of the craters in the range of 4 to 4.5 µm), whereas the highest wear was recorded for the uncoated insert, followed by CrAlNAg16 and CrAlNAg12 coated tools.

Due to running-in wear, the rate of crater wear was faster at the beginning, while it became steady subsequently as evident in Fig. 14. It may be further noted that although the coatings were partially removed from the chip sliding zone of the rake surface, the coated tools resulted in much higher tool life compared to their uncoated counterpart due to the "wear-pad effect." Moreover, it may be concluded that the results of high-temperature tribology, cutting forces and chip temperature had a strong correlation with the tool wear phenomena of the uncoated and developed CrAlNAg coatings.

The SEM images displayed in Fig. 15 illustrate the free and under surfaces of the chips after face milling of AISI 1045 steel using both uncoated and different coated tool inserts under the same cutting conditions. Generally, serrated or segmented chips are commonly observed during the machining of steels. The collected chips clearly exhibit the formation of serrated teeth during machining and the size of chip serration decreases when coated inserts were used. This reduction in chip separation size is a clear indication of better tool wear resistance and reduced shear stress while cutting with the coated inserts. The coating with the highest Ag content displays more pronounced serration as shown in Fig. 15.

The observed lamellar structure in Fig. 15 (a-f) is a fundamental feature of the free surface of the chips and characterised by jagged and rough appearances resulting from the shearing mechanism. In the major section of the chips, these lamellae align parallel with the side cutting edge, while in the corner section, they are inclined and roughly parallel with the nose of the tool. Similar observations have been reported by the previous researchers [52,53]. Fig. 15 (a_1-f_1) shows the under surfaces of the chips which were in sliding contact with the tool rake surface during milling operation. The undersurface indirectly represents the condition of chip-tool interface during machining. For example, rougher rake

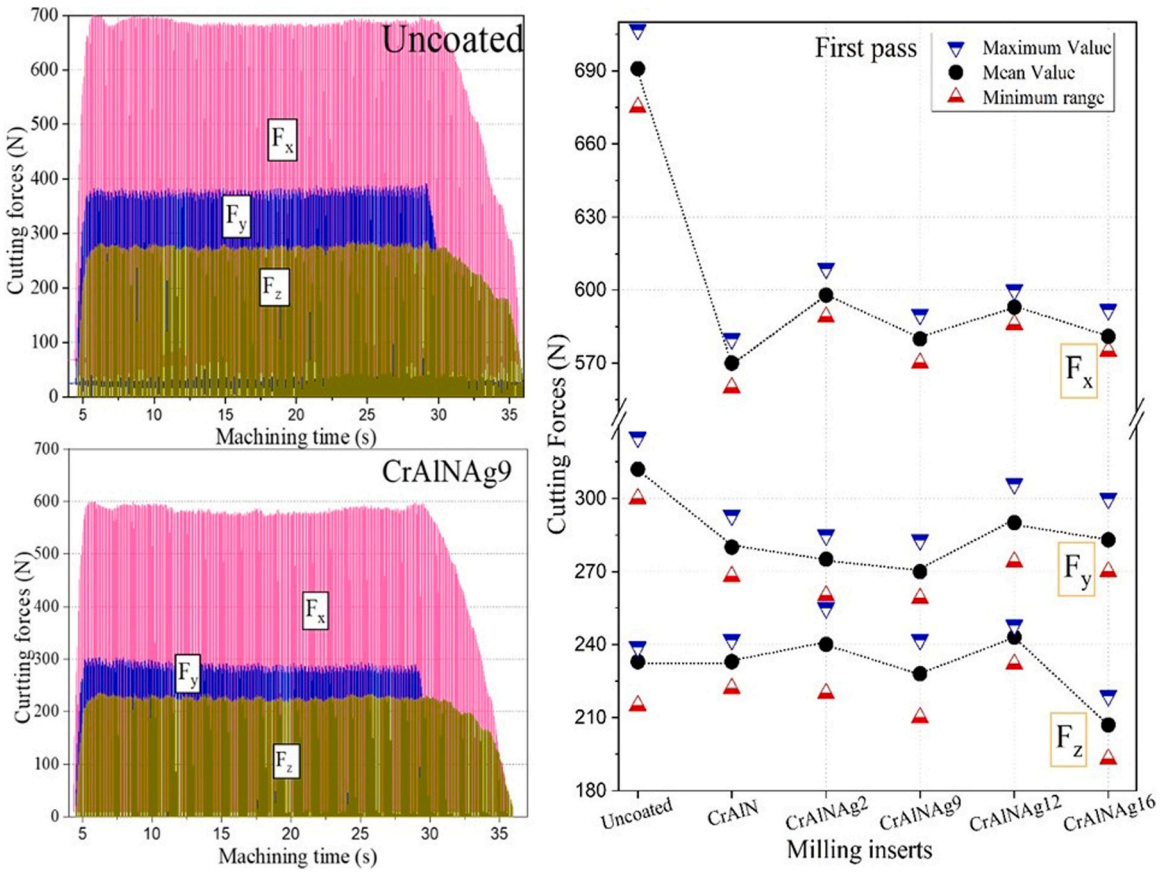

Fig. 10. Shows (a) representative cutting force signal during face milling of AISI 1045 steel using uncoated and CrAlNAg9 coated tools and (b) maximum, minimum and mean values of cutting forces using milling inserts under the condition of $V_c = 250$ m/min, $f_z = 0.3205$ mm/tooth, $a_p = 1$ mm, $a_e = 20$ mm.

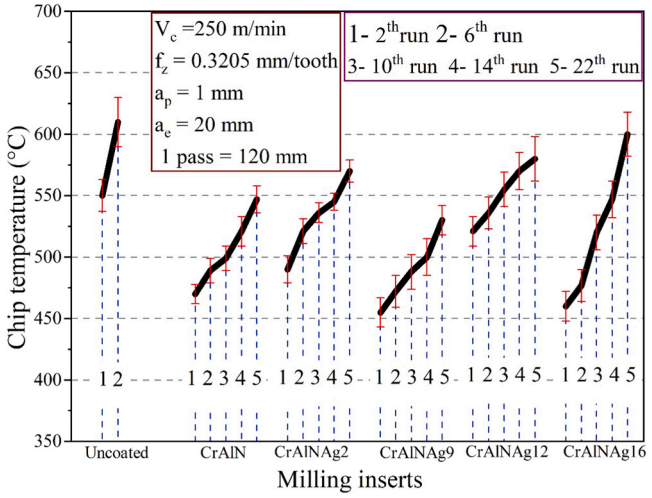

Fig. 11. Variation in chip temperature across machining runs during machining of 1045 steel using developed CrAlNAg coated tools.

surface morphology would induce some damage to the undersurface of the chip during machining. Tribochemical reactions such as oxidation at machining zone temperature also play a significant role in chip morphology.

During milling, similar to other cutting operations, the back surface of the chip encounters close contact with the tool rake face. During machining, severe plastic deformation of the chips takes place, resulting in elevated contact pressure and friction force. The cutting zone temperature is also considerably high, as shown in Fig. 11. The collective influence of high contact pressure, elevated temperature and frictional force contribute to a smooth and shiny back surface (see Fig. 15 (a_1-f_1)), in contrast to the free surface of the chips. Notably, parallel stripes on the undersurface are discernible, attributed to irregular cutting edges and/or potential hard particles; nevertheless, the overall surface remains smooth.

While the uncoated tool resulted in a smoother morphology of the undersurface of the chip, CrAlN-coated tool caused prominent abrasive marks. Moreover, the other coated inserts such as CrAlNAg2 and CrAlNAg12 showed inconsistency and tearing of the chips. Formation of harder phases like Al_2O_3 during tribological contact in machining might be responsible for the development of such a structure. It may be recalled that the formation of Al_2O_3 was detected inside the wear track during steel ball tribology test (Fig. 8), as well. However, for CrAlNAg9 and CrAlNAg16 coatings, softer phases are too dominant to cause major disruption in the back surface of the chip as evident from the figure. The R_a values of the rake surface were also connected to the morphology of the chip undersurface. For example, the uncoated and CrAlNAg9 coated tools with lower surface roughness than reference CrAlN coating resulted in smoother morphology of the back surface of the chips.

Fig. 16 shows the results of maximum chip thickness while using uncoated and different coated tools after the second run of milling operation. The same figure also includes the microscopic images of the chips. All the chips look similar as they are of discontinuous type with a C-shaped appearance. However, there is significant variation in the chip thickness as presented in the same figure. Since chip thickness is an indirect measure of mechanical deformation during machining, it is related to chip-tool interface friction and cutting force. The same figure depicts that the maximum chip thickness is recorded with the uncoated milling insert. Therefore, the cutting force results are coherent with

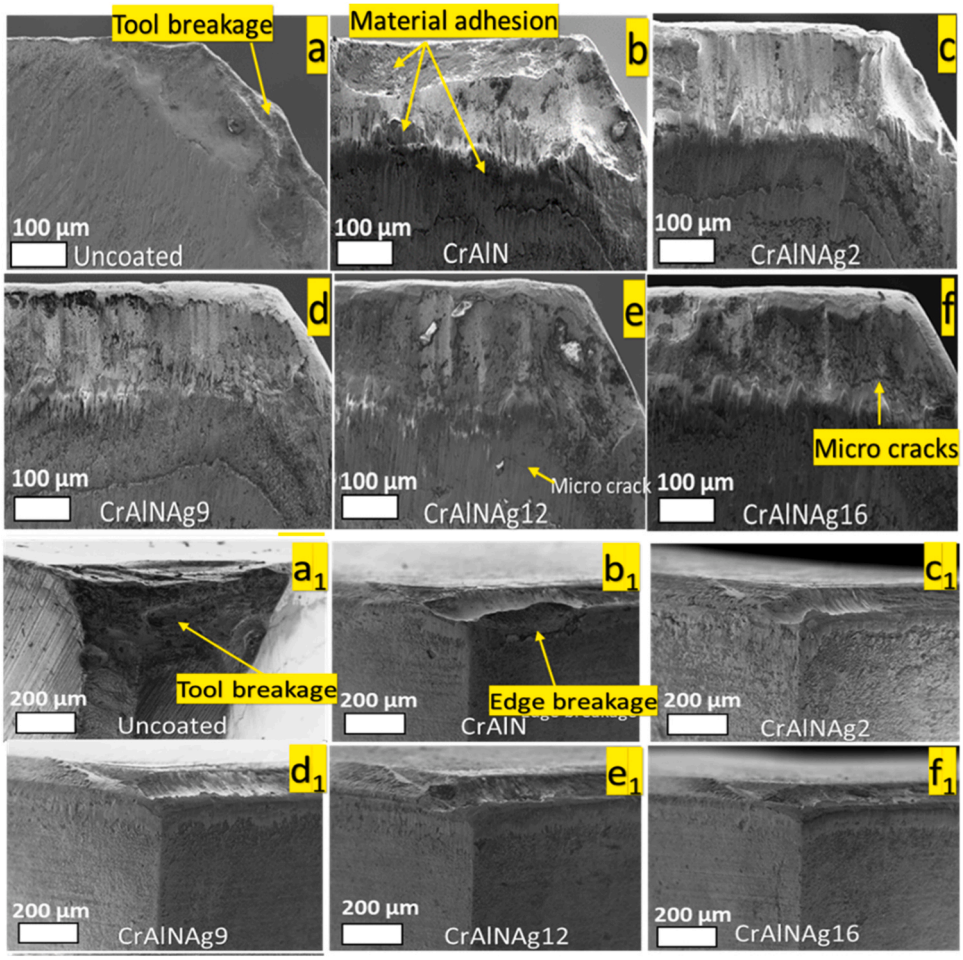

Fig. 12. SEM images of rake and flank surfaces of uncoated, developed CrAlNAg coated tools after 22 runs of milling operations under the condition of $V_c = 250$ m/min, $f_z = 0.3205$ mm/tooth, $a_p = 1$ mm, $a_e = 20$ mm.

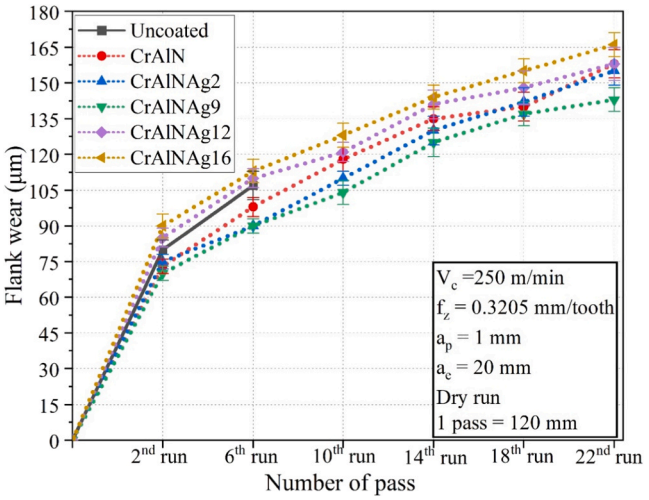

Fig. 13. Progression of average flank wear of uncoated, CrAlN and CrAlNAg coated tools during dry face milling operation.

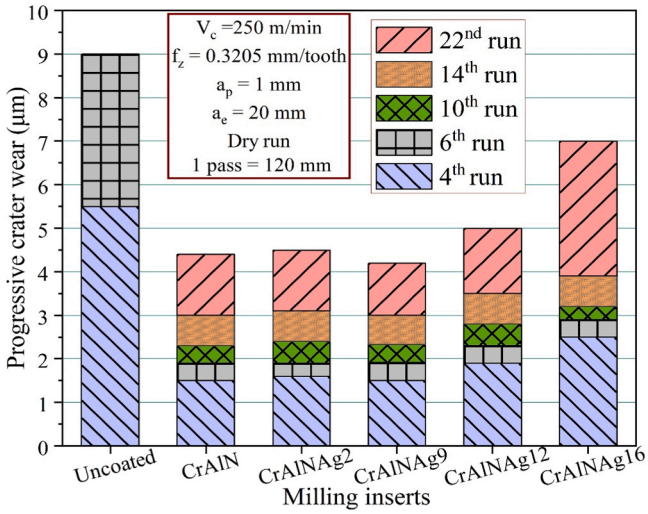

Fig. 14. Variation of progressive crater wear of uncoated and coated milling inserts during milling of AISI 1045 steel.

those of chip thickness, as the uncoated tool resulted in the highest values of F_x and F_y as shown in Fig. 10. Moreover, F_y and F_z (Fig. 10 (b)), related to the CrAlNAg9 coated tool, are either the smallest or second smallest respectively. Since the maximum chip thickness for the CrAlNAg9 coated tool is found to be minimum, it is evident that the same coating actually exhibits low friction characteristics during machining operation. It is also important to mention that the CrAlNAg12 coating resulted in the highest value of chip thickness among all the coated tools. This can be explained by the unfavourable formation of oxides in large quantities for the CrAlNAg12 coating during tribo-test, as presented in

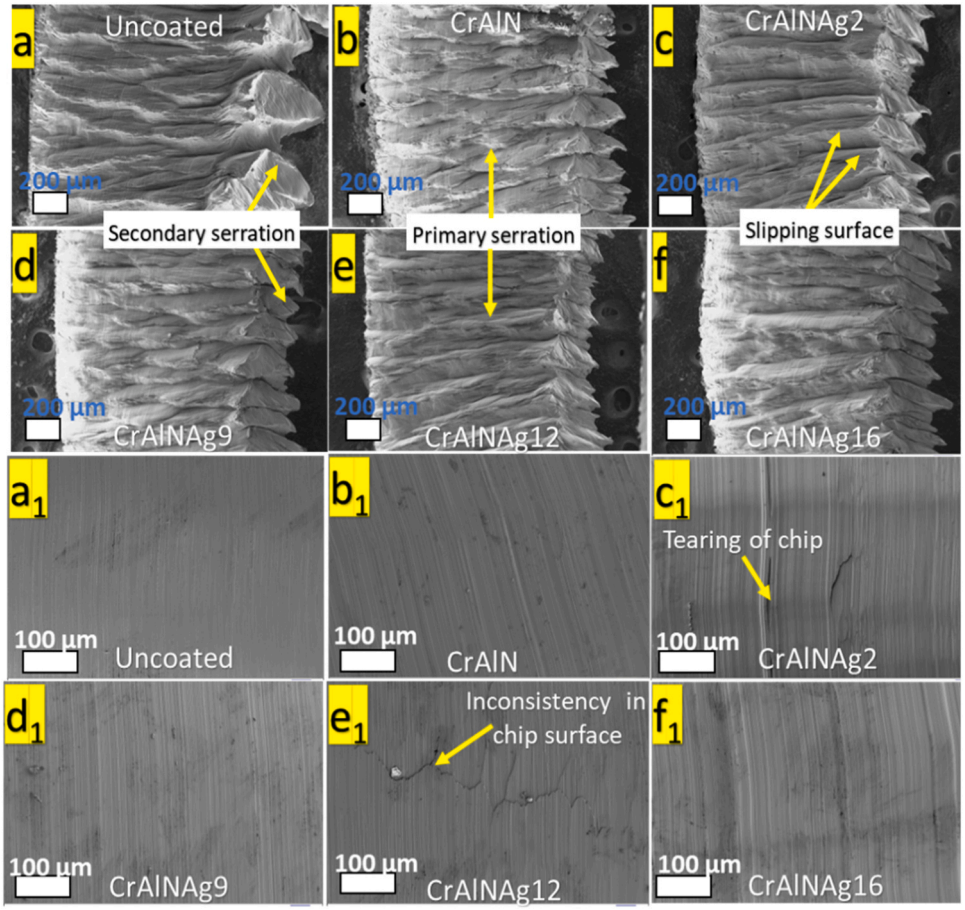

Fig. 15. SEM images of free and back surface of the chips while using uncoated, developed CrAlNAg coated milling inserts after machining under the condition of V_c = 250 m/min, f_z = 0.3205 mm/tooth, a_p = 1 mm, a_e = 20 mm.

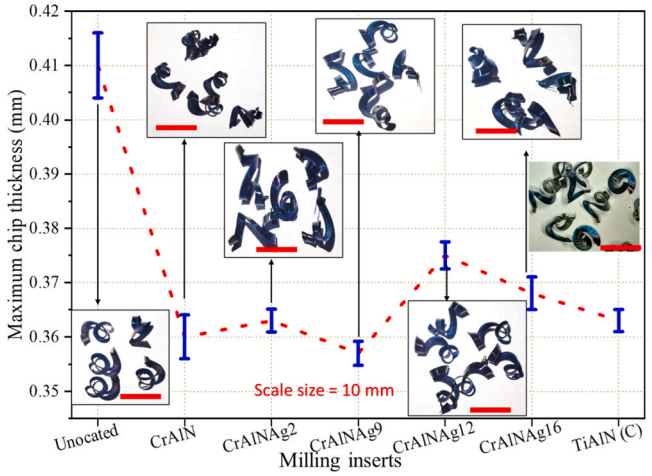

Fig. 16. Plot of maximum chip thickness after face milling operation while using uncoated, developed CrAlNAg coated tools.

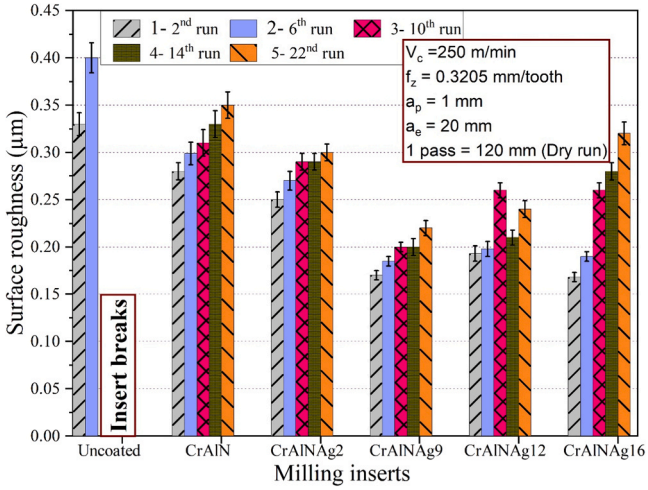

Fig. 17. Variation of surface roughness after different runs using uncoated and different coated milling inserts.

previous work [26].

The workpiece surface roughness after machining with uncoated and different coated tools is shown in Fig. 17. The results clearly highlight that the lowest surface roughness is initially achieved for CrAlNAg9 and CrAlNAg16 coatings. This indicates the effectiveness of the addition of Ag in the CrAlN coating. However, there is a significant increase in roughness observed for the CrAlNAg16 coating due to maximum flank and crater wear among the coated tools, as presented in Figs. 13 and 14.

Superior surface finish was obtained with the CrAlNAg9 coated tool (37–38 % improvement than reference CrAlN), which is attributed to its greater capability to prevent material adhesion on to the tool surface during machining. During ball-on-disk tribology test, the phenomenon of lower sticking tendency of CrAlNAg9 coating was clearly established (Figs. 4 and 6). Moreover, surface roughness is also directly correlated with tool wear as there is a clear increasing trend of surface roughness

with the progression of machining, as indicated in Fig. 17. Additionally, the rate of increase of roughness with machining runs is also correlated with the rate of tool wear. For example, uncoated and CrAlNAg16 coated tools exhibit a greater slope of increase of surface roughness compared to other coated tools.

4. Conclusion

During the ball-on-disk test at 600 °C, the steel ball counterpart softened and exhibited wear when sliding against CrAlN-based coatings without or lower content of Ag resulting in the development of wear flat. Moreover, these coatings demonstrated formation of a layer comprising worn particles of coating as well as ball counterparts in between. On the other hand, coatings with higher Ag content such as CrAlNAg9 and CrAlNAg12 helped in the formation of a protective transfer layer on the outer surface of the ball counterpart thereby mitigating the adhesion of wear debris onto the coated surface and wear of the steel ball. However, CrAlNAg16 coating with the highest Ag content displayed the formation of an unstable transfer layer on the counterpart, accompanied by a sizeable wear flat.

Both reference CrAlN and CrAlNAg9 coated tools were successful in reducing cutting force (F_x) by 17.5 % and 16 % respectively, with reference to the uncoated tool. The same CrAlN and CrAlNAg9 coated tools also diminished the chip temperature by 14.3 % and 17.5 % respectively, when compared to their uncoated counterpart. In a similar way, the same two coated tools caused a reduction in chip thickness by 12 % and 12.7 % with respect to the uncoated insert. However, no significant change in cutting forces, chip temperature and chip thickness could be observed while using CrAlNag9 and reference CrAlN coated tools. The effect of Ag addition was more prominent in the case of tool wear protection and machined surface roughness. CrAlNAg9 coated tool resulted in reduction in average flank wear in the range of 7 % to 10 % in comparison with the reference CrAlN coated tool. Under similar machining conditions, the uncoated milling insert could only survive an overall cutting length of 720 mm while all the coated tools were able to sustain a cutting length of 2640 mm without tool failure. CrAlNAg9 coated tool brought about decrease in surface roughness by ~47 % and ~36 % compared to uncoated and reference CrAlN coated tools, respectively. Superior surface finish was obtained with CrAlNAg9 coated tool (36–38 % improvement than the reference CrAlN) which is related to the anti-friction and anti-sticking properties provided by the transfer layer at the tribo-contact.

Statement of originality

The authors hereby declare that the manuscript entitled **"High-temperature tribological behaviour and machining performance of self-lubricant CAlNAg coatings for dry milling operations."** is an original work of the authors and this has not been submitted elsewhere for possible publication.

Declaration of Competing Interest

The authors declare that they have no known competing financial interests or personal relationships that could have appeared to influence the work reported in this paper.

Data Availability

The authors are unable or have chosen not to specify which data has been used.

Acknowledgments

The funding support received by Soumya Gangopadhyay from Department of Science and Technology, Government of India in relation to an international collaborative project (No. DST/INT/Portugal/P-14/2017) between India and Portugal. Filipe Fernandes acknowledges the UIDB/00285/2020 and LA/P/0112/2020 projects, sponsored by FEDER Funds through Portugal 2020 (PT2020), the Competitiveness and Internationalization Operational Program (COMPETE 2020), and national funds through the Portuguese Foundation for Science and Technology (FCT). Support received through the bilateral collaborative project (No. 441.00 INDIA) between Portugal and India is also thankfully acknowledged.

References

[1] Khanna N, Agrawal C, Pimenov DY, Singla AK, Machado AR, da Silva LRR, et al. Review on design and development of cryogenic machining setups for heat resistant alloys and composites. J Manuf Process 2021;68:398–422. https://doi.org/10.1016/j.jmapro.2021.05.053.

[2] Upadhyay C, Rajput SS, Kumar CS, Gangopadhyay S, Sahoo SK. Performance evaluation of WC, SiAlON and SiCw + Al_2O_3 tools in dry machining of Inconel 617. J Manuf Process 2024;109:235–49. https://doi.org/10.1016/j.jmapro.2023.12.006.

[3] Rajput S.S., Upadhyay C., Gangopadhyay S. Effects of roughing, finishing, and aggressive machining conditions on the milling performance of AISI 1045 steel using TiAlN coated inserts 2023. ⟨https://doi.org/10.1177/09544054231157963⟩.

[4] Salur E, Aslan A, Kuntoglu M, Gunes A, Sahin OS. Experimental study and analysis of machinability characteristics of metal matrix composites during drilling. Compos B Eng 2019;166:401–13. https://doi.org/10.1016/j.compositesb.2019.02.023.

[5] Kuntoğlu M, Sağlam H. Investigation of progressive tool wear for determining of optimized machining parameters in turning. Meas (Lond) 2019;140:427–36. https://doi.org/10.1016/j.measurement.2019.04.022.

[6] Yıldırım ÇV, Sarıkaya M, Kıvak T, Şirin Ş. The effect of addition of hBN nanoparticles to nanofluid-MQL on tool wear patterns, tool life, roughness and temperature in turning of Ni-based Inconel 625. Tribol Int 2019;134:443–56. https://doi.org/10.1016/j.triboint.2019.02.027.

[7] Gupta MK, Song Q, Liu Z, Sarikaya M, Jamil M, Mia M, et al. Environment and economic burden of sustainable cooling/lubrication methods in machining of Inconel-800. J Clean Prod 2021;287:125074. https://doi.org/10.1016/j.jclepro.2020.125074.

[8] Khanna N, Shah P, Chetan. Comparative analysis of dry, flood, MQL and cryogenic CO_2 techniques during the machining of 15-5-PH SS alloy. Tribol Int 2020;146:106196. https://doi.org/10.1016/j.triboint.2020.106196.

[9] Sivaiah P, Chakradhar D. Effect of cryogenic coolant on turning performance characteristics during machining of 17-4 PH stainless steel: A comparison with MQL, wet, dry machining. CIRP J Manuf Sci Technol 2018;21:86–96. https://doi.org/10.1016/j.cirpj.2018.02.004.

[10] Zhao J, Liu Z, Wang B, Song Q, Ren X, Wan Y. Effects of Al content in TiAlN coatings on tool wear and cutting temperature during dry machining IN718. Tribol Int 2022;171:107540. https://doi.org/10.1016/j.triboint.2022.107540.

[11] Chubb JP, Billingham J, Hall DD, Walls JM. Comparison of wear behaviour of single- and multilayer coated carbide cutting tools. Met Technol 1980;7:293–9. https://doi.org/10.1179/030716980803286559.

[12] Schintlmeister W, Pacher O. Preparation and Properties of Hard-Material Layers for Metal Machining and Jewelry. J Vac Sci Technol 1975;12:743–8. https://doi.org/10.1116/1.568659.

[13] Jafari M, Rogström L, Andersson JM, Birch J, Gibmeier J, Jöesaar MJ, et al. Thermal degradation of TiN and TiAlN coatings during rapid laser treatment. Surf Coat Technol 2021;422. https://doi.org/10.1016/j.surfcoat.2021.127517.

[14] Biava G, de Araujo Fernandes Siqueira IB, Vaz RF, de Souza GB, Jambo HCM, Szogyenyi A, et al. Evaluation of high temperature corrosion resistance of CrN, AlCrN, and TiAlN arc evaporation PVD coatings deposited on Waspaloy. Surf Coat Technol 2022;438:128398. https://doi.org/10.1016/j.surfcoat.2022.128398.

[15] Yoon SY, Lee KO, Kang SS, Kim KH. Comparison for mechanical properties between TiN and TiAlN coating layers by AIP technique. J Mater Process Technol 2002;130–131:260–5. https://doi.org/10.1016/S0924-0136(02)00746-X.

[16] Chim YC, Ding XZ, Zeng XT, Zhang S. Oxidation resistance of TiN, CrN, TiAlN and CrAlN coatings deposited by lateral rotating cathode arc. Thin Solid Films 2009;517:4845–9. https://doi.org/10.1016/j.tsf.2009.03.038.

[17] Reiter AE, Derflinger VH, Hanselmann B, Bachmann T, Sartory B. Investigation of the properties of $Al_{1-x}Cr_xN$ coatings prepared by cathodic arc evaporation. Surf Coat Technol 2005;200:2114–22. https://doi.org/10.1016/j.surfcoat.2005.01.043.

[18] Ding X, Tan ALK, Zeng XT, Wang C, Yue T, Sun CQ. Corrosion resistance of CrAlN and TiAlN coatings deposited by lateral rotating cathode arc. Thin Solid Films 2008;516:5716–20. https://doi.org/10.1016/j.tsf.2007.07.069.

[19] Varghese V, K. A, Ramesh MR, Chakradhar D. Investigation on the performance of AlCrN and AlTiN coated cemented carbide inserts during end milling of maraging steel under dry, wet and cryogenic environments. J Manuf Process 2019;43:136–44. https://doi.org/10.1016/j.jmapro.2019.05.021.

[20] Drnovšek A, Kukuruzović D, Terek P, Miletić A, Čekada M, Panjan M, et al. Microstructural, mechanical and oxidation resistance of nanolayer sputter-deposited CrAlN hard coatings. Coatings 2023;13. https://doi.org/10.3390/coatings13122096.

[21] Lee KK, Kim HS, Ahn DG, Lee H. Thermo-mechanical characteristics of inconel 718 layer deposited on AISI 1045 steel substrate using a directed energy deposition process. J Mater Res Technol 2022;17:293–309. https://doi.org/10.1016/j.jmrt.2021.12.112.
[22] Bondarev AV, Kvashnin DG, Shchetinin IV, Shtansky DV. Temperature-dependent structural transformation and friction behavior of nanocomposite VCN-(Ag) coatings. Mater Des 2018;160:964–73. https://doi.org/10.1016/j.matdes.2018.10.029.
[23] Fernandes F, Al-Rjoub A, Cavaleiro D, Polcar T, Cavaleiro A. Room and high temperature tribological performance of multilayered tisin/tin and tisin/tin(Ag) coatings deposited by sputtering. Coatings 2020;10:1–13. https://doi.org/10.3390/coatings10121191.
[24] Dang C, Li J, Wang Y, Yang Y, Wang Y, Chen J. Influence of Ag contents on structure and tribological properties of TiSiN-Ag nanocomposite coatings on Ti–6Al–4V. Appl Surf Sci 2017;394:613–24. https://doi.org/10.1016/j.apsusc.2016.10.126.
[25] Al-Rjoub A, Cavaleiro A, Rajput SS, Fernandes F. High Si multilayered TiSiN/TiN (Ag) films with superior oxidation resistance. J Mater Res Technol 2021;12:2340–7. https://doi.org/10.1016/j.jmrt.2021.04.040.
[26] Rajput SS, Gangopadhyay S, Yaqub TB, Cavaleiro A, Fernandes F. Room and high temperature tribological performance of CrAlN(Ag) coatings: The influence of Ag additions. Surf Coat Technol 2022;450. https://doi.org/10.1016/j.surfcoat.2022.129011.
[27] Mulligan CP, Gall D. CrN-Ag self-lubricating hard coatings. Surf Coat Technol 2005;200:1495–500. https://doi.org/10.1016/j.surfcoat.2005.08.063.
[28] Basnyat P, Luster B, Kertzman Z, Stadler S, Kohli P, Aouadi S, et al. Mechanical and tribological properties of CrAlN-Ag self-lubricating films. Surf Coat Technol 2007;202:1011–6. https://doi.org/10.1016/j.surfcoat.2007.05.088.
[29] Rajput SS, Bhangale A, Moharana A, Gangopadhyay S, Ferreira F, Fernandes F. Effect of Ag addition on the oxidation behavior of CrAlN coating at elevated temperatures. Mater Today Proc 2023. https://doi.org/10.1016/j.matpr.2023.06.337.
[30] Mulligan CP, Blanchet TA, Gall D. CrN-Ag nanocomposite coatings: High-temperature tribological response. Wear 2010;269:125–31. https://doi.org/10.1016/j.wear.2010.03.015.
[31] Kutschej K, Mitterer C, Mulligan CP, Gall D. High-temperature tribological behavior of Cr'N-Ag self-lubricating coatings. Adv Eng Mater 2006;8:1125–9. https://doi.org/10.1002/adem.200600131.
[32] Incerti L, Rota A, Valeri S, Miguel A, García JA, Rodríguez RJ, et al. Nanostructured self-lubricating CrN-Ag films deposited by PVD arc discharge and magnetron sputtering. Vacuum 2011;vol. 85:1108–13. https://doi.org/10.1016/j.vacuum.2011.01.022.
[33] Ren P, Zhang K, He X, Du S, Yang X, An T, et al. Toughness enhancement and tribochemistry of the Nb-Ag-N films actuated by solute Ag. Acta Mater 2017;137:1–11. https://doi.org/10.1016/j.actamat.2017.07.034.
[34] Rajput SS, Gangopadhyay S, Cavaleiro A, AL-Rjoub A, Kumar CS, Fernandes F. Influence of Ag additions on the structure, mechanical properties and oxidation behaviour of CrAlNAg coatings deposited by sputtering. Surf Coat Technol 2021;426:127767. https://doi.org/10.1016/j.surfcoat.2021.127767.
[35] Ye F, Lou Z, Wang Y, Liu W. Wear mechanism of Ag as solid lubricant for wide range temperature application in micro-beam plasma cladded Ni60 coatings. Tribol Int 2022;167. https://doi.org/10.1016/j.triboint.2021.107402.
[36] Lin J, Li C-L, Lee J-W, Zhang X, Xiao J, Piper SC. Development and evaluation of CrAlAgN self-lubricating coatings for high temperature metal forming dies. J Vac Sci Technol A 2024;42. https://doi.org/10.1116/6.0003306.
[37] Egaña A, Rech J, Arrazola PJ. Characterization of Friction and Heat Partition Coefficients during Machining of a TiAl6V4 Titanium Alloy and a Cemented Carbide. Tribology Trans 2012;55:665–76. https://doi.org/10.1080/10402004.2012.692007.
[38] Qasim A, Nisar S, Shah A, Khalid MS, Sheikh MA. Optimization of process parameters for machining of AISI-1045 steel using Taguchi design and ANOVA. Simul Model Pr Theory 2015;59:36–51. https://doi.org/10.1016/j.simpat.2015.08.004.
[39] Ye GG, Xue SF, Ma W, Jiang MQ, Ling Z, Tong XH, et al. Cutting AISI 1045 steel at very high speeds. Int J Mach Tools Manuf 2012;56:1–9. https://doi.org/10.1016/j.ijmachtools.2011.12.009.
[40] Liu C, He Y, Wang Y, Li Y, Wang S, Wang L, et al. Effects of process parameters on cutting temperature in dry machining of ball screw. ISA Trans 2020;101:493–502. https://doi.org/10.1016/j.isatra.2020.01.031.
[41] Stott FH, Jordan MP. The effects of load and substrate hardness on the development and maintenance of wear-protective layers during sliding at elevated temperatures. Wear 2001;250–251:391–400. https://doi.org/10.1016/S0043-1648(01)00601-9.
[42] Ghiotti A, Bruschi S, Borsetto F. Tribological characteristics of high strength steel sheets under hot stamping conditions. J Mater Process Technol 2011;211:1694–700. https://doi.org/10.1016/j.jmatprotec.2011.05.009.
[43] Stott FH. High-temperature sliding wear of metals. Tribol Int 2002;35:489–95. https://doi.org/10.1016/S0301-679X(02)00041-5.
[44] Hernandez S, Hardell J, Winkelmann H, Ripoll MR, Prakash B. Influence of temperature on abrasive wear of boron steel and hot forming tool steels. Wear 2015;338–339:27–35. https://doi.org/10.1016/j.wear.2015.05.010.
[45] Stott FH, Glascott J, Wood GC. Models for the Generation of Oxides During Sliding Wear. Proc R Soc Lond Ser A, Math Phys Sci 1985;402:167–86. ⟨http://www.jstor.org/stable/2397802⟩.
[46] Wu YP, Chiang HY, Hsiang HI. $AgCrO_2$ formation mechanism during silver inner electrode and Fe–Si–Cr alloy powder co-firing in metal multilayer chip power inductors. J Mater Sci: Mater Electron 2019. https://doi.org/10.1007/s10854-019-01130-5.
[47] Calderon VS, Cavaleiro A, Carvalho S. Chemical and structural characterization of Zr-C-N-Ag coatings: XPS, XRD and Raman spectroscopy. Appl Surf Sci 2015;346:240–7. https://doi.org/10.1016/j.apsusc.2015.03.161.
[48] Cavaleiro D, Cavaleiro A, Carvalho S, Fernandes F. Oxidation behaviour of TiSiN (Ag) films deposited by high power impulse magnetron sputtering. Thin Solid Films 2019;688:137423. https://doi.org/10.1016/j.tsf.2019.137423.
[49] Hu JJ, Muratore C, Voevodin AA. Silver diffusion and high-temperature lubrication mechanisms of YSZ-Ag-Mo based nanocomposite coatings. Compos Sci Technol 2007;67:336–47. https://doi.org/10.1016/j.compscitech.2006.09.008.
[50] Papi PA, Mulligan CP, Gall D. CrN-Ag nanocomposite coatings: Control of lubricant transport by diffusion barriers. Thin Solid Films 2012;524:211–7. https://doi.org/10.1016/j.tsf.2012.10.010.
[51] Varela LB, Cavaleiro A, Tschiptschin AP, Gangopadhyay S, Fernandes F. Tribological and milling performance of NbC–Ni films deposited by sputtering with different Ni contents. Tribol Int 2020;147:106281. https://doi.org/10.1016/j.triboint.2020.106281.
[52] Zhang S, Guo YB. An experimental and analytical analysis on chip morphology, phase transformation, oxidation, and their relationships in finish hard milling. Int J Mach Tools Manuf 2009;49:805–13. https://doi.org/10.1016/j.ijmachtools.2009.06.006.
[53] Zhao Y, Sun J, Li J. Study on chip morphology and milling characteristics of laser cladding layer. Int J Adv Manuf Technol 2015;77:783–96. https://doi.org/10.1007/s00170-014-6483-2.